Radioimmunotherapy with radioactive nanoparticles: Biological doses and treatment efficiency for vascularized tumors with or without a central hypoxic area

V. Bouchat[a] and V. E. Nuttens
Research Center in Physics of Matter and Radiation (PMR), Laboratoire d'Analyses par Réactions Nucléaires (LARN), University of Namur (FUNDP), Rue de Bruxelles 61, B-5000 Namur, Belgium

C. Michiels
Unité de Recherche en Biologie Cellulaire (URBC), University of Namur (FUNDP), Rue de Bruxelles 61, B-5000 Namur, Belgium

B. Masereel
Department of Pharmacy (DP), University of Namur (FUNDP), Rue de Bruxelles 61, B-5000 Namur, Belgium

O. Feron
Unité de Pharmacothérapie (FATH), Université Catholique de Louvain (UCL), Avenue Mounier 53, B-1200 Brussels, Belgium

B. Gallez
Laboratoire de Resonance Magnétique Biomédicale (CMFA), Université Catholique de Louvain (UCL), Avenue Mounier 73, B-1200 Brussels, Belgium

T. Vander Borght
Center for Molecular Imaging and Experimental Radiotherapy (IRME), Université Catholique de Louvain (UCL), Dr. G. Therasse 1, B-5530 Yvoir, Belgium

S. Lucas
Research Center in Physics of Matter and Radiation (PMR), Laboratoire d'Analyses par Réactions Nucléaires (LARN), University of Namur (FUNDP), Rue de Bruxelles 61, B-5000 Namur, Belgium

(Received 7 September 2009; revised 23 February 2010; accepted for publication 1 March 2010; published 29 March 2010)

Purpose: Radioactive atoms attached to monoclonal antibodies are used in radioimmunotherapy to treat cancer while limiting radiation to healthy tissues. One limitation of this method is that only one radioactive atom is linked to each antibody and the deposited dose is often insufficient to eradicate solid and radioresistant tumors. In a previous study, simulations with the Monte Carlo N-Particle eXtended code showed that physical doses up to 50 Gy can be delivered inside tumors by replacing the single radionuclide by a radioactive nanoparticle of 5 nm diameter containing hundreds of radioactive atoms. However, tumoral and normal tissues are not equally sensitive to radiation, and previous works did not take account the biological effects such as cellular repair processes or the presence of less radiosensitive cells such as hypoxic cells.
Methods: The idea is to adapt the linear-quadratic expression to the tumor model and to determine biological effective doses (BEDs) delivered through and around a tumor. This BED is then incorporated into a Poisson formula to determine the shell control probability (SCP) which predicts the cell cluster-killing efficiency at different distances "*r*" from the center of the tumor. BED and SCP models are used to analyze the advantages of injecting radioactive nanoparticles instead of a single radionuclide per vector in radioimmunotherapy.
Results: Calculations of BED and SCP for different distances *r* from the center of a solid tumor, using the non-small-cell lung cancer as an example, were investigated for $^{90}Y_2O_3$ nanoparticles. With a total activity of about 3.5 and 20 MBq for tumor radii of 0.5 and 1.0 cm, respectively, results show that a very high BED is deposited in the well oxygenated part of the spherical carcinoma.
Conclusions: For either small or large solid tumors, BED and SCP calculations highlight the important benefit in replacing the single β-emitter ^{90}Y attached to each antibody by a $^{90}Y_2O_3$ nanoparticle. © *2010 American Association of Physicists in Medicine*. [DOI: 10.1118/1.3368599]

Key words: shell control probability (SCP), biological effective dose (BED), radioimmunotherapy, dosimetry, Monte Carlo, tumor model, nanomedicine

I. INTRODUCTION

In radioimmunotherapy (RIT), cancer cells are killed thanks to potential induction of immune response and to ionizing radiation delivered by single radionuclides coupled to antibodies. The radiation efficacy is mainly influenced by the choice of the radioactive atom linked to each antibody as well as the biokinetics and the biodistribution of radiolabeled antibodies used to target a human tumor antigen. Clinical studies have, however, shown that doses higher than 60–70 Gy inside tumors are required for treating solid and poorly vascularized cancers.[1] Such doses are not easily obtained with such an approach, in spite of numerous efforts made to increase antibody accumulation and penetration inside the tumor.[2–5]

In a previous paper, we have proposed improving the tumor dose deposition, and therefore, the treatment response by replacing the single radioactive atom bound to each monoclonal antibody (mAb) by a 5 nm diameter inorganic nanoparticle composed of numerous radioactive and nonradioactive atoms.[6] The aim of such a treatment is to deliver a much higher dose to the tumor. Moreover, inorganic nanoparticles can contain different types of radionuclides (α, β, γ, or x-ray emitters) suited to both diagnostic and therapeutic applications.[7] The possible mix between different radiations will thus represent a practical tool for theragnostics.[8] This kind of radiolabeled antibody do not exist yet, but the development of both organic and inorganic nanoparticles that specifically target tumor cells or cancer vasculature has received considerable interest these past few years. Progress has been made to improve the stability of these nanoparticles within a biological microenvironment.[7] For example, by creating spherical radioactive nanoparticles whose diameter does not exceed 5 nm, the radiolabeled antibodies are small enough to reduce the opsonization process by the reticuloendothelial system (RES) responsible for their rapid clearance from blood circulation.[9] To avoid that any radioactive atom come off of the nanoparticle, it is possible to cover the nanoparticles with a thin layer of inert and biocompatible matter, such as Au or C. These biocompatible surfaces could also be coated by polymeric macromolecules, such as polyethylene glycol. This type of macromolecule enhances the chemical stability of nanoparticles in an aqueous environment and can act as a protective layer against the RES.[7,9–13] Finally, nanoparticles of 5 nm diameter possess a large surface capable of accommodating large number of functional groups so that more than one antibody can be conjugated per particle. The more antibodies per nanoparticles there are, the higher will be the biological half-life and uptake. Indeed, *in vivo* imaging on animals and humans has shown that targeted nanoparticles can be preferentially distributed in tumor mass after injection and relatively low accumulation of these nanoparticles is observed in other organs such as the spleen or liver, which means that antibodies can well be used to target the nanoparticles to specific anatomical sites.[7,14–16]

Beta-emitting radioactive nanoparticles have already been created and investigated with promising results. For example, researchers at the University of Missouri-Columbia have developed an efficient methodology to synthesize radioactive gold nanoparticles (12–18 nm) containing ^{198}Au β-emitters (β_{max}=0.96 MeV; half-life of 2.7 days). Coated with gum arabic (polysaccharide glycoprotein), they did not observe any aggregation or decomposition of these ^{198}Au nanoparticles in saline solution. Moreover, glycoprotein molecules have receptors in the liver and biodistribution studies performed on mice clearly showed a significant localization of ^{198}Au nanoparticles in liver.[17,18] Finally, therapeutic efficacy was tested on mice bearing a model of human prostate cancer. An uptake of NPs in prostate cancer cells and a decrease in the tumor volume are clearly observed after a direct injection into the solid tumor.[19] More recently, Wu and co-workers[20] proposed synthesizing radioactive nanoparticles of ^{90}Y by using a protein cage of apoferritin. First tests were performed by diffusing ^{89}Y and phosphate ions into the cavity of apoferritin. The diameter of these phosphate/apoferritin nanoparticles was around 8 nm after functionalization.

Despite these promising results to produce radioactive nanoparticles for radioimmunotherapy, a question remains: What would be the benefit of such configuration involving antibodies labeled with several ^{90}Y atoms configured as nanoparticles in term of dose and tumor control. This paper attempts to answer to that question with the help of Monte Carlo simulations and a simple ^{90}Y configuration.

Monte Carlo N-Particle eXtended (MCNPX) simulations have been used to evaluate the physical dose around and throughout a spherical solid tumor. Dosimetry calculations were performed for the beta-emitting radionuclide $^{90}Y_2O_3$ and preliminary results showed that viable tumor cells receive physical doses of up to 50 Gy everywhere inside the tumor. This observation is still valid even for large nonuniform distribution of the total activity inside the tumor. Moreover, dose deposited around the tumor remains sufficiently weak to avoid affecting the surrounding healthy tissues.[6] However, the efficacy of a treatment against cancer does not depend only on the physical absorbed doses but also on other radiobiological parameters such as the radiosensitivity of the targeted tissues, the doubling time of the cancer cells, the repair process of sublethal damage taking place between two irradiations, and the effect of hypoxia for which the radiosensitivity changes according to whether cells are anoxic or well oxygenated.[21–23] All these biological effects are taken into account in the biological effective dose (BED) and tumor control probability (TCP) models. Consequently, they offer interesting tools to evaluate, at least theoretically, the efficacy of a specific treatment. Moreover, these mathematical models are often used to compare different radiotherapy techniques and to predict the most appropriate treatment for individual patients.[24–28]

In this work, BED and control probability for successive concentric spherical shells inside and around the tumor [shell control probability (SCP)] have been calculated for the non-small-cell lung cancer (NSCLC). This type of tumor is a good example of carcinomas for which patients have poor survival.[29,30] Indeed, this cancer is relatively radioresistant and displays important hypoxic areas. Doses larger than

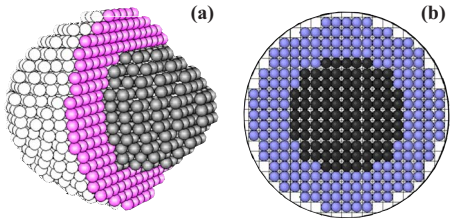

FIG. 1. Spherical tumor of 0.5 cm radius subdivided into 3591 cell clusters. (a) The first picture is a three-dimensional arrangement of these cell clusters when 25% of the cell clusters are poorly oxygenated at the center of the tumor. Picture (b) corresponds to a cross-section of the center of this modelized tumor with cell clusters inside a cubic lattice of 500 μm width.

60–70 Gy are thus required to cure NSCLC.[1,30,31] In radioimmunotherapy, doses up to 60 Gy can be delivered within the tumor after several injections of radiolabeled antibodies over several days or weeks. Unfortunately, NSCLC is also well-known to be fast growing, with a cell doubling time ranging from 2.5 to 3.3 days.[1] So it is better to deliver a high total dose during a single injection rather than in small fractions over a longer time. In external beam therapy, such doses can be deposited at the tumor in one session but a great part of the surrounding healthy tissues will be also irradiated. In these conditions, RIT using radioactive nanoparticles coupled to an antibody seems to be a good method for treating solid carcinomas such as the NSCLC, since a single injection will be able to deliver doses larger than 60–70 Gy to the targeted tumor. It is, however, important to verify whether doses to healthy lung tissue remain lower than 30 Gy to avoid late complications like pneumonitis or fibrosis.[1,22,29] In the present paper, the physical doses $D(r)$ previously simulated with MCNPX 5.0 are converted into BED and SCP distributions. The main objective is, then, to analyze the cell cluster-killing efficiency resulting from the use of antibodies coupled to radioactive nanoparticles and compare these results to BED and SCP calculations when a single β-emitter ^{90}Y is coupled to each antibody.

II. BED AND SCP CALCULATIONS

II.A. Tumor model

Absorbed doses as a function of distance from the center of the tumor were simulated according to the MCNPX 2.5.0 code. This Monte Carlo software requires accurate information on the tumor structure and the microscopic distribution of radioactivity delivered by the radiolabeled antibodies. In order to accurately provide such information, we developed a new model for a spherical vascularized tumor in which the antibody distributions inside the tumor are uniform or heterogeneous. This tumor model is described in detail in a previous publication and consists of a set of spherical cell clusters of 250 μm radius arranged in a simple cubic lattice structure as illustrated in Fig. 1.[6] The spherical tumor of 0.5 cm radius can contain a maximum number of 3591 cell clusters. When the spherical tumor has a radius of 1.0 cm, the number of cell clusters increases to a value of 31 071 (Table I). The matter around each cell cluster represents the vascularized stroma containing a pre-existing blood network or new vessels created during angiogenesis. The radiolabeled antibodies can penetrate inside the tumor through this vasculature to surround the various cell clusters. The distribution of radiolabeled antibodies inside the tumor is uniform if all cell clusters in the cubic lattice have the same probability to be reached by an antibody. However, it is well-known that during angiogenesis, the outer region of the tumor is better vascularized than the center.[32–34] The density of blood vessels decreases toward the center and the heterogeneity in blood flow thus generates a nonuniform distribution of radioactivity in tumors.[35] In order to take this decrease in vasculature into account, linear and exponential distributions of radiolabeled antibodies inside the tumor have been modelized by subdividing the tumoral sphere into concentric shells of 0.05 cm thickness, with differing probabilities to be reached by an antibody. In our model, the probability that an antibody reaches a cell cluster located near the tumor radius hits a maximum value of 1.0. Inversely, the probability decreases to 0.1 for antibodies which reach the central cell cluster of the tumor. Between those values, the probability may decrease linearly [Eq. (1)] or exponentially [Eq. (2)].

$$LP(m) = 0.1 + \left(\frac{1.0 - 0.1}{\text{NbShell} - 1}\right) \times (m - 1), \quad (1)$$

TABLE I. Parameters used for calculating the total activity inside tumors of different radii (0.5 and 1.0 cm) when antibodies are linked with radioactive nanoparticles or with single ^{90}Y atoms.

		R_T=0.5 cm		R_T=1.0 cm	
Parameters	Units	NP of ^{90}Y	Single ^{90}Y	NP of ^{90}Y	Single ^{90}Y
Total # of cell clusters	···	3591	3591	31 071	31 071
Hypoxic radius	cm	0.32	0.32	0.64	0.64
# of nonhypoxic cell clusters	···	2702	2702	23 342	23 342
Physical half-life	h	64.1	64.1	64.1	64.1
Biological half-life	h	72	72	72	72
Covering fraction	mAb/cm^2	3.8×10^7	10^{10}	2.5×10^7	10^{10}
# of ^{90}Y per MAb	···	1000	1	1000	1
Calculated total activity	MBq	3.5	0.9	20	7.5

$$EP(m) = \exp\left[\ln(0.1) + \left(\frac{\ln(1.0) - \ln(0.1)}{\text{NbShell} - 1}\right) \times (m - 1)\right], \quad (2)$$

where NbShell represents the total number of shells obtained by subdividing the tumor radius by the thickness of concentric shells. "*m*" may vary from 1 for the cell cluster located at the center of the tumor to Nbshell for the cell clusters located in the vicinity of the tumor surface.

Furthermore, it has to be noted that the center of large tumors often displays poorly oxygenated or hypoxic cells caused by the lack of vasculature. This situation can lead to the formation of a necrosed core. Central hypoxic areas are introduced in our tumor model by simply considering that the probability that an antibody reaches this region is null. The radius of the hypoxic core can vary widely with time and tumor type. In this work, we have chosen radii of 0.32 and 0.64 cm for both tumor radii of 0.5 and 1.0 cm, respectively. In this case, numbers of hypoxic cell clusters are 889 for the first tumor and 7729 for the second, meaning that about 25% of the total number of cell clusters are not oxygenated (dark gray cell clusters in Fig. 1). Radii of hypoxic cores and numbers of normally oxygenated cell clusters are given in Table I for tumors of 0.5 and 1.0 cm radii.

II.B. Absorbed dose calculations

This tumor model was used to calculate the deposited dose inside and around cancer cells as a function of the distance from the center for two tumor radii (0.5 and 1.0 cm). In these simulations, tumors were irradiated by $^{90}Y_2O_3$ nanoparticles of 5 nm diameter. A 5 nm diameter nanoparticle of $^{90}Y_2O_3$ can contain a maximum of 1.73×10^3 atoms of yttrium-90, but we assume that the delay time between the antibodies' injection and their binding with tumoral antigens is 2 days, which means that only 60% of radioactive atoms inside each nanocluster are still radioactive when the nanoclusters reach the cancer cells.

Energy deposition for different distances "*r*" from the tumor center was determined by using SMESH tally proposed in the MCNPX code. The latter is capable of studying the electron transport through matter by taking into account the loss of energy, multiple scattering angles and "bremsstrahlung." All these physical processes are considered by using the photon-electron mode and the default PHYS cards for electron and photons with a cutoff energy at 0.005 MeV for both particles. The number of histories (NPs) was set to 50×10^6 particles and β spectral data for yttrium-90 was taken from tables on the RADAR site (www.doseinfo-radar.cp/RADARDecay.html). The SMESH tally builds virtual three-dimensional spherical grids superimposed on the geometry of our tumor model and gives the energy deposition, in MeV/g per emitted particle, into each concentric spherical shell independently of the composition or density of each material used to modelize the tumor and its surrounding tissues. This energy deposition is then converted into deposited doses $D(r)$, in Gy, by the formula (3) proposed by Nuttens[36]

$$D(r) = 21.34 \times E(r) \times p \times \tilde{A}/\lambda_{\text{eff}}, \quad (3)$$

where $E(r)$ is the energy deposition at a distance r from the center of the tumor, p is the average number of electrons emitted per disintegration, λ_{eff} $(=\ln(2)/T_{1/2}^{\text{eff}})$ is the effective decay constant, assuming a monoexponential decay.[37] λ_{eff} is given by the sum of the physical decay and the biological clearance rate constants $(\lambda_{\text{eff}}=\lambda_{\text{phy}}+\lambda_{\text{biol}})$.[6,36] The physical half-life of yttrium-90 is well-known and corresponds to 64.1 h.[38–40] Based on pharmacokinetic studies on ^{90}Y, Wiseman and co-workers[41] estimated that the biological blood half-life of the antibody varies between 22 and 140 h. For our simulation, we supposed a biological half-life for healthy tissues of about 72 h.[42,43] Clearance of the antibodies inside the tumor must be slower than in healthy tissues. But due to the short physical half-life of yttrium-90, the biological half-life in the tumor is mainly determined by the physical half-life of yttrium-90. So, for our simulations, we also supposed a biological half-life of 72 h for tumor tissues. In these conditions, the effective decay constant (λ_{eff}) was evaluated at 2.04×10^{-2} h^{-1} both for healthy tissues and tumors. The total activity $\tilde{A}$ was calculated according to the expression (4) given in a previous publication[6]

$$\tilde{A} = \lambda_{\text{phys}} \times n_u \times n_a \times n_{\text{mAb}}, \quad (4)$$

where n_u and n_a represent, respectively, the number of nonhypoxic tumor cell clusters and the number of radioactive atoms per nanoparticle (Table I). n_{mAb} is the quantity of monoclonal antibodies which surrounds each cell cluster. Its value was calculated by multiplying the surface of the cell cluster by the covering fraction defined as the number of bound mAbs per unit of tumor surface. The covering fraction was adjusted to ensure a maximal dose of 30 Gy around the tumor surface. In our model, this value is reached if covering fractions are 3.8×10^7 and 2.5×10^7 mAb/cm^2 for solid tumors of 0.5 and 1.0 cm radii, respectively. These values are clearly lower than typical values for covering fractions given for monoclonal antibodies coupled to a single radionuclide, which range from 10^8 to 10^{10} mAb/cm^2.[39] With parameters listed in Table I, we calculated the total activity according to Eq. (4) above. The latter represents the activity that would be injected directly into tumors. When the radioactive nanoclusters are used, the total activities are about 3.5 MBq for tumor of 0.5 cm radius and 20 MBq for tumor of 1.0 cm radius. These values are very large if we compare them to cumulated activities obtained when a single ^{90}Y atom is linked to each antibody. Indeed, despite of a maximal covering fraction of 10^{10} mAb/cm^2, total activities for single ^{90}Y per mAb decrease to 0.9 and to 7.5 MBq for tumor radii of 0.5 and 1.0 cm, respectively. These total activities (Table I) will be used to compute the TCP and SCP.

The thickness between each spherical mesh was reduced to 0.05 cm to increase the number of shells inside and around the tumor. This value is less than 1 mm, which is the minimal thickness normally imposed by the software MCNPX 2.5.0.[44,45] In order to test the influence of shell thicknesses on deposited energies simulated by MCNPX, a comparison

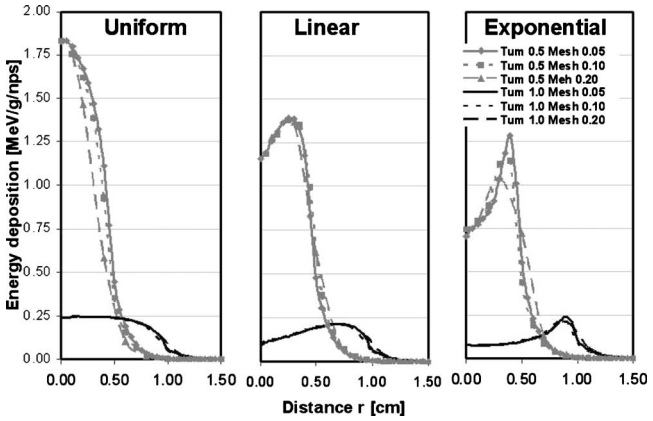

FIG. 2. Effect of the thickness of concentric spherical shells on energy deposition (per gram and per emitted particle) for tumors with radii of 0.5 and 1.0 cm: 0.5 (solid lines), 1.0 (dotted lines), and 2.0 mm (dashed lines). Uniform, linear, and exponential distributions of antibodies are taken into account.

among three different segmentations of concentric spherical shells (0.5, 1.0, and 2.0 mm) was performed. As shown in Fig. 2 for tumors of 0.5 cm radius, the three curves representing the energy deposition for the three different thicknesses display great disparities. When the activity is uniformly dispersed throughout the tumor, deposited energies simulated with MCNPX tend to decrease in tumoral and normal tissues with the number of concentric spherical shells. For linear distribution of antibodies, predicted deposited energy inside the tumor is diminished when the number of segmentations decreases, whereas it increases in healthy tissues. Finally, curves plotted for the exponential distribution of antibodies show an increase and a shift in the peak toward the right when the thickness between meshes decreases. It is worth noting that these differences in simulated energy deposition according to the choice of the segmentation disappear for a larger tumor radius. Indeed, as illustrated in Fig. 2 for a tumor with a radius of 1.0 cm, curves of deposited energies are similar whatever the thickness of concentric spherical shells, especially for uniform and linear antibody distribution. When the antibodies are distributed exponentially, an increase in the maximal dose deposited near the tumor surface is observed when the thickness between concentric spherical shells decreases. Consequently, the nature of the mesh chosen to simulate energy deposition may have an incidence on the shape of the predicted absorbed dose distribution curve for small tumor radii. The segmentation of 0.05 cm was chosen to provide more points on the energy deposition curve and because linear or exponential probability decreases for each cell cluster to be reached by antibodies have also been done by steps of 0.05 cm. The latter corresponds to the diameter chosen for cell cluster constituting the tumor.[6]

II.C. BED(r), error, and SCP(r) calculations

BED distribution and TCP are adequate methods to analyze the radiobiological effects of treatment resulting from radioactive nanoparticles. Both BED and TCP distributions are mathematical models often used to predict the response to irradiation of normal and tumor tissues, which is very useful for evaluating the best treatment for each individual patient.[25,42,46] Absorbed doses $D(r)$ were thus converted into BED according to Eq. (5) given by

$$\mathrm{BED}(r) = \frac{D(r)}{q} + \frac{\lambda_{\mathrm{eff}}}{(\lambda_{\mathrm{eff}} + \mu)} \frac{D(r)^2}{q^2 \alpha/\beta}. \tag{5}$$

In our model, a spherical tumor is subdivided in cell clusters and BED(r) is defined as the dose required for killing a cell unit located at a distance r from the center of the tumor. $D(r)$ is the absorbed dose computed by our MCNPX simulations. λ_{eff}, μ, α/β, and q are biological parameters (see hereunder). This equation is valid for both tumors and healthy tissues, but differences exist between radiobiological factors for tumoral and normal tissues. The values of these parameters for the three antibody distributions are presented in Table II. The choice of these values is explained in the following two paragraphs.

All terms in Eq. (5) have a biological significance. Ionizing radiation can affect living tissues on a cellular level by

TABLE II. Biological parameters and their references used for BED and SCP calculations for tumor and healthy tissues.

	Tumor			Healthy tissues		
Biological factors	Range values	Tumoral tissues	Error	Range values	Healthy tissues	Error
$T_{\mathrm{bio}}^{1/2}$ (h)	22–140[a]	72	±24	22–140[a]	72	±24
α/β (Gy)	>5 [b–d]	10[e–g,b,h]	±5	≤5 [b–d]	3[e–g,b,h]	±2
μ (h^{-1})	0.3–2.5[b,i]	1.39[b,h]	±0.5	0.3–2.5[b,i]	0.46[g,b,j]	±0.5
ρ (#/cm^3)	10^7–10^8	5×10^7 [k]	…	10^7–10^8	5×10^7 [k]	…
α (Gy^{-1})	0.1–1.0[l]	0.35[e]	…	…	0.031[m]	…

[a]Reference 41.
[b]Reference 49.
[c]Reference 58.
[d]Reference 59.
[e]Reference 1.
[f]Reference 22.
[g]Reference 42.
[h]Reference 51.
[i]Reference 53.
[j]Reference 54.
[k]Reference 60.
[l]Reference 37.
[m]Reference 61.

breaking chemical bonds within DNA molecules. The linear term in expression (5) refers to single ionizing events, which directly provoke double-strand breaks in DNA. This kind of damage, also called type A damage by Dale and co-workers,[47,48] is necessarily lethal because it is not repairable. Inversely, the quadratic component describes the cellular death as a consequence of two separated sublethal damages (type B damage) and these damages can be repaired when the lapsed time between the two hits is long enough.[26,37,47,49–52] The ratio $\lambda_{eff}/(\lambda_{eff}+\mu)$ was incorporated in the expression to take into account the reduction in cell destruction due to repair of sublethal damage during continuous irradiation.[26,47,51,52] This term is deduced from the dose protraction factor for continuous irradiation ($T=\infty$) and varies between 0 and 1. $\mu(=\ln(2)/T_{1/2}^{Rep})$ is the exponential rate constant that quantifies the rate of sublethal damage repair. The half-time of DNA repair ($T^{1/2}_{Rep}$) for normal and tumor tissues may range from a few minutes to several hours.[49,53] In our simulation, calculations have been performed with a $T^{1/2}_{Rep}$ of 1.5 h for healthy tissues, which is the repair half-time most widely adopted by authors.[42,49,54] The corresponding repair constant μ is then 0.46 h^{-1}. For a solid tumor, a lower repair half-time of 0.5 h is generally proposed for simulations, giving a repair constant μ of 1.4 h^{-1}.[49,51] This higher value of μ limits the chance of producing lethal damage by interaction with a second hit, thus reducing the overall treatment efficacy. Also called cellular radiosensitivity, α and β are tissue specific parameters expressed in Gy^{-1} and Gy^{-2}, respectively. Both parameters are determined by a fit of the cell survival curves.[27,49,55–57] The α/β ratio gives an indication of the relative importance of the linear and quadratic terms and determines the shape of the cell survival curve. It is well recognized that α/β ratios less or equal to 5 Gy are generally observed for late-responding tissue. Inversely, values higher than 5 Gy are observed for a majority of tumors.[49,58,59] For our simulations, values of 3 and 10 Gy were chosen for normal and tumoral tissues, respectively, because they are the most often used values.[1,22,42,49,51]

In our tumor model, we have introduced the possibility of having a hypoxic core. In these conditions, all cell clusters at the center of the tumor are less radiosensitive than those which are well oxygenated.[21–23,55] So, to differentiate α and β values for poorly and normally oxygenated cell clusters, the "q" parameter was introduced. This parameter, also called hypoxia reduction factor, was first proposed by Jones and co-workers[62] to calculate BED for hypoxic cells. They supposed that the radiosensitivity coefficient α and β for a specific tissue are reduced, respectively, by q and q^2 when cells are hypoxic. Indeed, experimental studies have shown that poorly vascularized areas are up to three times more resistant to ionizing radiation than proliferating cells.[30,62] So, the simplest model is to assume that q is equal to 1 when cells are well oxygenated and to 3 when cells are hypoxic.

The biological parameters are strongly dependent on the structure, the shape, and the cellular composition of a tumor. Experimental evaluations of these radiobiological parameters often lead to variable values. For our simulations, we simply took the most recurrent values proposed in the literature. In order to evaluate the impact of variation in these biological parameters on BED distributions, errors in BED were calculated according to Eq. (6)

$$\Delta\mathrm{BED}=\frac{\partial\mathrm{BED}}{\partial(\alpha/\beta)}\Delta(\alpha/\beta)+\frac{\partial\mathrm{BED}}{\partial\mu}\Delta\mu+\frac{\partial\mathrm{BED}}{\lambda_{eff}}\Delta\lambda_{eff}+\frac{\partial\mathrm{BED}}{\partial D}\Delta D. \tag{6}$$

The last term $(\partial\mathrm{BED}/\partial D)\Delta D$ is negligible because D is computed to the point that ΔD is minimal. Since $\Delta\lambda_{eff}=\Delta\lambda_{bio}+\Delta\lambda_{phys}$ and $\Delta\lambda_{phys}$ is negligible compared to $\Delta\lambda_{bio}$, then

$$\Delta\lambda_{eff}=-\frac{\ln 2}{T_{bio}^2}\Delta T_{bio}. \tag{7}$$

Values for $\Delta(\alpha/\beta)$, $\Delta\mu$, and ΔT_{bio} used to calculate ΔBED are presented in Table II (column 4 for tumor and column 7 for healthy tissues). Partial derivatives are determined by

$$\frac{\partial\mathrm{BED}}{\partial(\alpha/\beta)}=\frac{\lambda}{\lambda+\mu}\cdot\frac{\dot{D}_0^2}{\lambda^2}\cdot\frac{-1}{(\alpha/\beta)^2}, \tag{8}$$

$$\frac{\partial\mathrm{BED}}{\partial\mu}=\frac{-\lambda}{(\lambda+\mu)^2}\cdot\frac{1}{(\alpha/\beta)}\cdot\frac{\dot{D}_0^2}{\lambda^2}, \tag{9}$$

$$\frac{\partial\mathrm{BED}}{\partial\lambda_{eff}}=-\frac{\dot{D}_0^2}{\lambda^2}+\frac{-1}{(\lambda^2+\lambda\mu)^2}\cdot\frac{1}{(\alpha/\beta)}\cdot\dot{D}_0^2\cdot(2\lambda+\mu). \tag{10}$$

BED(r) distributions calculated according to Eq. (5) will be used to determine SCP(r), which is defined as the probability that no cell cluster inside each spherical mesh located at a distance r from the center of the tumor survives irradiation. SCP(r) is based on the TCP-NTCP concept. Indeed, SCP(r) is capable of predicting the survival rate of cell clusters after irradiation inside the tumor but, also, in the surrounding healthy tissues. The control probability for a single cell cluster inside a spherical shell located at a distance r from the center of the tumor defined by the SMESH tally was first calculated. Cell clusters are assumed to be dead when all clonogenic cells inside the aggregate are killed by single or double hit events. As TCP, this probability can be calculated using the Poissonian form expressed by[28,37,49]

$$\mathrm{CCP}(r\pm\Delta r)\approx\exp\{-N\cdot\exp\{-\alpha\cdot\mathrm{BED}(r)\}\}, \tag{11}$$

where CCP($r\pm\Delta r$) is the cluster control probability of a cell cluster located at a distance $r\pm\Delta r$ from the center of the tumor, Δr representing the small variations between the distance separating the cluster from the tumor center and the real distance r of the spherical shell defined by the SMESH tally. N is the number of cells before irradiation inside each cube defined by the cubic lattice of 500 μm length sides used to subdivide the tumor sphere. The cell density is assumed to be uniform throughout the tumor and healthy tissues. So, with a value of 5×10^7 cell/cm^3, the number N of cells in each cube of the cubic lattice corresponds to 6250.[60]

TABLE III. Calculated values of D (in Gy), BED (in Gy), and ΔBED (in %) for a tumor of 0.5 cm radius with or without hypoxia according to data in Tables I and II. For each antibody distribution (uniform, linear, and exponential), the table gives the maximum doses deposited inside the tumor (Max), doses at the center (Cent), doses at the surface (Surf), and 1 mm beyond the surface (Out) of the tumor. Data are calculated for a single ^{90}Y atom labeled antibody and for a radioactive nanoparticle labeled antibody.

		Tumor of 0.5 cm radius											
		Single radionuclide total activity: 0.9 MBq						Radioactive nanoparticle total activity: 3.5 MBq					
		No hypoxia			25% hypoxic			No hypoxia			25% hypoxic		
		D (Gy)	BED (Gy)	ΔBED (%)	D (Gy)	BED (Gy)	ΔBED (%)	D (Gy)	BED (Gy)	ΔBED (%)	D (Gy)	BED (Gy)	ΔBED (%)
Uniform	**Cent**	44	47	6	16	5	1	173	217	18	63	21	3
	Max	45	47	6	35	36	5	173	217	18	135	162	15
	Surf	11	11	2	12	12	2	42	45	6	48	51	6
	Out	5	5	6	5	6	7	18	22	20	20	26	21
Linear	**Cent**	28	29	4	13	4	1	110	128	12	51	17	2
	Max	34	35	5	33	34	5	132	157	14	127	150	14
	Surf	12	12	2	13	14	2	45	48	6	53	57	7
	Out	5	5	7	6	6	8	19	24	21	22	29	23
Exponential	**Cent**	28	29	4	12	12	1	67	73	8	48	16	2
	Max	34	35	5	32	34	4	122	144	14	126	149	14
	Surf	12	12	2	14	14	2	53	57	7	55	59	7
	Out	5	5	7	6	6	8	22	28	23	23	30	23

Equation (11) requires a defined value of α and not only the α/β ratio. This is probably the most difficult radiobiological factor to determine because it is clearly dependent on the patient and the type of tumor. Atthey and co-workers[37] proposed that plausible values for α may range from 0.1 to 1.0 Gy^{-1}. For non-small-cell lung cancer, α parameter may vary between 0.3 and 0.4 Gy^{-1}.[1] So, we have chosen a mean value of 0.35 Gy^{-1} for calculating BED and CCP. A lower value of 0.031 Gy^{-1} was used for the α parameter of healthy lung tissues according to Dubray and co-workers.[61] Finally, shell control probability for the three different radiolabeled antibody distributions (uniform, linear, and exponential) is defined by the following product:

$$\mathrm{SCP}(r) = \prod_{i}^{K} \mathrm{CCP}_i(r \pm \Delta r), \tag{12}$$

where K represents the number of cell clusters in each spherical shell defined by the SMESH tally. The TCP can be then calculated by the product of all SCP(r) values, with r varying from 0 (center of the tumor) to r_T (surface of the tumor).

$$\mathrm{TCP} = \prod_{r=0}^{r=r_T} \mathrm{SCP}(r). \tag{13}$$

III. RESULTS AND DISCUSSION

Results presented in this work highlight the advantages of replacing a single radionuclide per antibody with inorganic nanoparticles containing a high number of radioactive atoms. BED(r) and SCP(r) were determined according to Eqs. (5) and (12), which take into account the effects of inhomogeneous dose distributions, cellular repair effects between two single-hit events, and the influence of a radioresistant hypoxic core within the tumor. We investigated whether the nature of the spatial distribution of antibodies and the presence of a hypoxic center affect the level of damage caused to cancer cells and to the cells in the surrounding tissue. Effects of repopulation in normal and tumor tissues will be ignored because they are less important than damage repair effects during continuous irradiation.[63] BED was calculated for two spherical tumors of 0.5 and 1.0 cm radii irradiated by 5 nm diameter nanoparticles of $^{90}Y_2O_3$. Results are summarized in Table III for tumor radius of 0.5 cm and in Table IV for tumor radius of 1.0 cm. They present values for physical doses $D(r)$ computed with MCNPX, biological effective doses calculated with Eq. (5), and errors on BED(r) due to variations in biological parameters, obtained from Eq. (6) and expressed in %.

Tables III and IV resume the most important values for the physical and biological doses inside and outside the tumor. The first are the D and the BED values at the center of the tumor, written down "Cent" in the second column of tables. When this center is well irradiated with doses of up to 60 Gy, the complete destruction of the tumor would be possible. In the second column, we can also find "Max" which gives the maximum values, which can be deposited within the tumors. To analyze the impact of the radiolabeled nanoparticles on healthy tissues, the value of D and BED at the surface of the tumor (Surf) and 1 mm beyond the tumor surface (Out) are also given. The best situation is to obtain a high physical or biological dose at the tumor surface where the proliferation is probably the most important and a minimum value for D or BED in the surrounding healthy tissues. Finally, values of D and BED at the center, at the surface and 1 mm beyond the tumor surface, as well as the maximum physical and biological doses deposited inside the tumor are

TABLE IV. Calculated values of D (in Gy), BED (in Gy), and ΔBED (in %) for a tumor of 1.0 cm radius with or without hypoxia according to data in Tables I and II. For each antibody distribution (uniform, linear, and exponential), the table gives the maximum doses deposited inside the tumor (Max), doses at the center (Cent), doses at the surface (Surf), and 1 mm beyond the surface (Out) of the tumor. Data are calculated for a single ^{90}Y atom labeled antibody and for a radioactive nanoparticle labeled antibody.

		Tumor of 1.0 cm radius											
		Single radionuclide total activity: 7.5 MBq						Radioactive nanoparticle total activity: 20 MBq					
		No hypoxia			25% hypoxic			No hypoxia			25% hypoxic		
		D (Gy)	BED (Gy)	ΔBED (%)	D (Gy)	BED (Gy)	ΔBED (%)	D (Gy)	BED (Gy)	ΔBED (%)	D (Gy)	BED (Gy)	ΔBED (%)
Uniform	**Cent**	51	54	7	3	1	1	132	157	14	7	2	1
	Max	51	56	7	51	55	7	135	162	15	132	158	14
	Surf	13	13	2	16	17	3	33	34	5	42	45	6
	Out	6	7	8	8	9	10	16	20	18	21	27	22
Linear	**Cent**	25	26	4	1	0	1	49	52	6	3	1	<1
	Max	45	48	6	50	54	6	117	137	13	131	156	14
	Surf	15	15	2	19	20	3	38	40	5	50	54	6
	Out	7	12	9	10	11	12	19	24	20	25	34	25
Exponential	**Cent**	17	17	3	1	0	1	44	46	6	2	1	<1
	Max	50	54	6	54	59	7	131	156	14	141	170	15
	Surf	22	23	3	24	25	4	57	62	7	62	67	8
	Out	11	12	13	12	14	14	28	39	27	30	43	29

calculated for a tumor with or without a hypoxic core and for the three types of antibody distributions: Uniform, linear, and exponential.

III.A. BED distributions for tumors without hypoxia

III.A.1. Nanoparticle labeled antibody

Figures 3 and 4 show a comparison between absorbed (solid gray lines) and biological (solid black lines) dose distributions for nonhypoxic tumors with a radius of 0.5 or 1.0 cm after injection of radioactive nanoparticles of 5 nm diameter containing $^{90}Y_2O_3$ distributed uniformly, linearly, or exponentially. A comparison between the three graphs of Figs. 3 and 4 shows that types of antibody distribution (uniform, linear, or exponential) in tumors affect noticeably the shape of absorbed and biological dose distributions, generating lower or higher doses at different distances from tumor center. However, the overall shape of the physically absorbed dose curve is similar to that of biological dose and this is true for each antibody distribution. The conversion of physical doses into BED shows higher values for doses inside the tumor, especially at the center when antibodies are dispersed uniformly. At this position, a difference of about 45 and 30

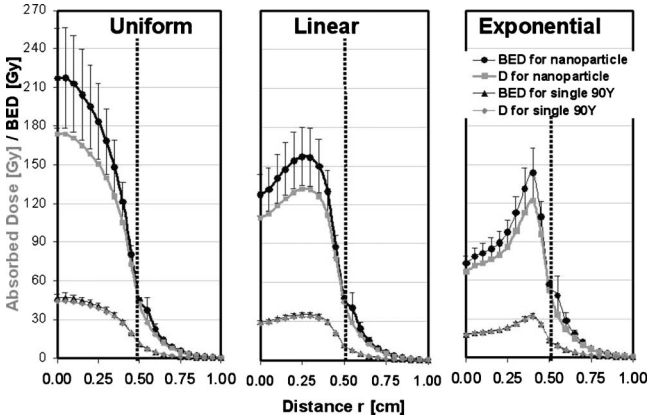

FIG. 3. Comparison of $D(r)$ and BED(r) profiles for $^{90}Y_2O_3$ nanoparticle labeled antibodies and for single ^{90}Y labeled antibodies, in Gray unit, as a function of the distance r from center for tumor with a radius of 0.5 cm and for three different antibodies distributions: Uniform, linear, and exponential. The tumors do not have hypoxic cores and dotted vertical lines represent the tumor radius. Solid black curves for all spectra are BED(r) and solid gray curves are $D(r)$ doses. Values for BED(r) were determined according to parameters given in Table II and Eq. (5) with $q=1$ for both tumor and healthy tissues.

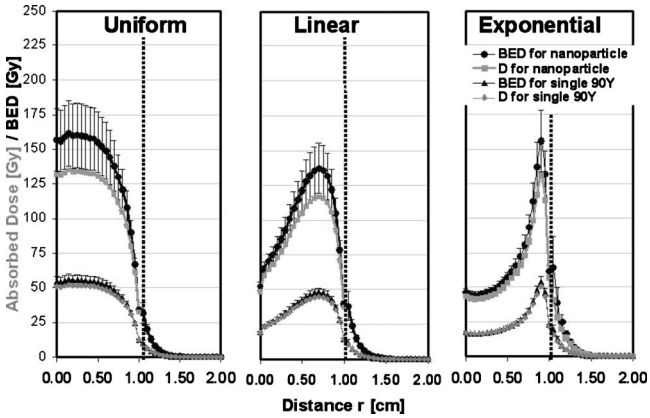

FIG. 4. Comparison of $D(r)$ and BED(r) profiles for $^{90}Y_2O_3$ nanoparticle labeled antibodies and for single ^{90}Y labeled antibodies, in Gray unit, as a function of the distance r from center for tumor radius with a radius of 1.0 cm and for three different antibodies distributions: Uniform, linear, and exponential. The tumors do not have hypoxic cores and dotted vertical lines represent the tumor radius. Solid black curves for all spectra are BED(r) and solid gray curves are $D(r)$ doses. Values for BED(r) were determined according to parameters given in Table II and Eq. (1) with $q=1$ for both tumor and healthy tissues.

Gy is observed between the absorbed dose and the biological dose for tumors of 0.5 and 1.0 cm radii, respectively. This increase is clearly due to the presence of the quadratic component of the calculated BED. For the linear or exponential distributions of antibodies, maximum peaks are observed at 0.25 or 0.40 cm for a tumor radius of 0.5 cm and at 0.70 or 0.90 cm when the tumor radius reaches 1.0 cm. These maximum doses are clearly located near the tumoral surface where the cell proliferation is the most important. For both tumor radii, BED(r) at 1 mm beyond the tumoral surface (i.e., in healthy tissue) remains inferior to 30 Gy, except for the exponential distribution of antibodies for the 0.1 cm radius tumor where the biological dose reaches 39 Gy. This last result highlights how significantly radiolabeled nanoparticles penetrate deeply inside the tumor rather than staying in the vicinity of the surface. Indeed, the more the distribution is exponential, the more that dose deposition inside healthy tissues is important. It is also possible to use radionuclides with shorter emission ranges to increase the sharpness of the falloff near the surface of the tumor on the absorbed dose and the biological dose curves.

As there exist uncertainties in the values for different biological parameters proposed in literature, error bars on biological dose curves have been added to see how the variation in μ and α/β can influence initial BED values (Figs. 3 and 4). The difference between biological and absorbed doses is strongly dependent on the choice of radiobiological factors. The decrease or increase in BED values is mainly due to variations in the repair half-time (T_μ) parameter. For a tumor of 0.5 cm radius, an increase in T_μ values from 0.5 to 1.5 h generates an increase in BED maximal values from 217 to 301 Gy, from 157 to 205 Gy, or from 144 to 185 Gy for uniform, linear, or exponential antibody distributions, respectively. Such an observation makes sense because cells with higher repair half-time for sublethal damage have a higher probability of undergoing cell death after an interaction with a second radiation. BED values are also weakly reduced when α/β increases. If a α/β ratio of 15 Gy is used in the model instead of 10 Gy, the maximal BED value for a tumor of 0.5 cm radius changes from 217 to 203 Gy, from 157 to 148 Gy, and from 144 to 136 Gy for uniform, linear, or exponential antibody distributions, respectively. The fact that BED values are reduced is logical because a diminution in the α/β ratio induces a decrease in the quadratic term of Eq. (5). However, BED values in healthy tissues are lower than BED inside the tumor, although values of μ and α/β are about three times less than in normal tissues.

All these results demonstrate how important it is to know, with accuracy, the biodistribution of antibodies and the biological factors when BED is calculated inside the tumor. However, with values up to 60 Gy everywhere inside the tumor, biological doses required to treat a cancer remain sufficient even if α/β or μ varies within a plausible range of values. Moreover, in most cases, BED values lower than 30 Gy are observed in surrounding healthy tissues indicating that they will be spared. However, all these values are probably underestimated because the presence of antibodies in healthy tissues in this model is assumed to be null. Furthermore, error bars for BED in healthy tissues are small, which means that large variations in biological parameters induce small differences of BED. Such findings are important to ensure the patient safety.

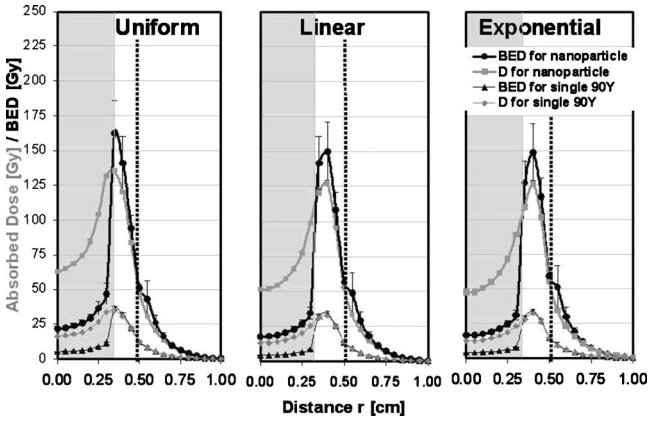

FIG. 5. Comparison of $D(r)$ and BED(r) profiles for $^{90}Y_2O_3$ nanoparticle labeled antibodies and for single ^{90}Y labeled antibodies, in Gray unit, as a function of the distance r from center for a tumor radius with a radius of 0.5 cm, for three different antibodies distribution: Uniform, linear, and exponential. The gray parts symbolize the hypoxic core of 0.32 cm radius and dotted vertical lines represent the tumor radius. Values for BED(r) were determined according to parameters given in Table II and Eq. (5) with $q=1$, with the exception that the value of q changes from 1 to 3 for the hypoxic core.

III.A.2. Single atom labeled antibody

Previous results have to be compared to dosimetry calculations when only a single radionuclide ^{90}Y is coupled to each antibody. To determine absorbed doses, the maximal covering fraction of 10^{10} mAbs/cm^2 has been considered.[39] With such a value, total activities correspond to about 0.9 and 7.5 MBq for tumors of 0.5 and 1.0 cm radii, respectively. As illustrated in Fig. 3 for a tumor of 0.5 cm radius, differences between D and BED curves are smaller than those observed for radioactive nanoparticles. Moreover, absorbed and biological doses are inferior to 60 Gy, which means that the activity deposited by radiolabeled antibodies is insufficient to correctly treat solid tumors such as non-small-cell lung carcinomas. This result remains true independently of the type of antibody distribution. Similar results are obtained for a tumor with a radius of 1.0 cm (Fig. 4) despite the larger total activity. Without hypoxia, values of absorbed and biological doses vary between 20 and 60 Gy for the three different antibody distributions, which is again insufficient to obtain good treatment outcome.

III.B. BED distributions for tumors with hypoxia

The presence of a large central hypoxia in the tumor can greatly influence clinical outcome in targeted radiotherapy. As explained earlier, our tumor model is capable of taking into account two types of cells with different radiosensitivity: Normally oxygenated ($q=1$) and hypoxic cells ($q=3$). BEDs were modelized for tumors of 0.5 and 1.0 cm radii containing a hypoxic core (Figs. 5 and 6). The percentage of hy-

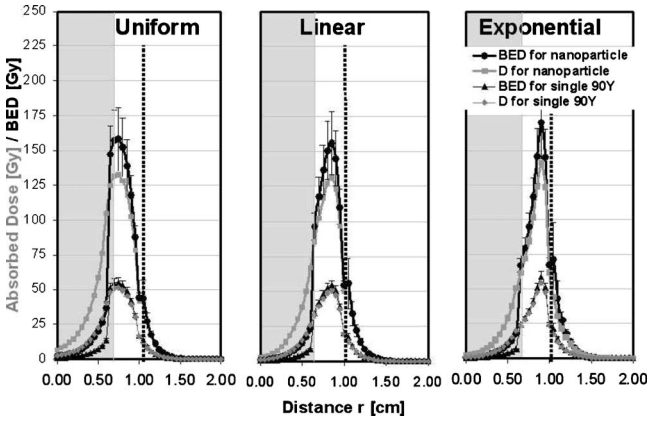

FIG. 6. Comparison of $D(r)$ and BED(r) profiles for $^{90}Y_2O_3$ nanoparticle labeled antibodies and for single ^{90}Y labeled antibodies, in Gray unit, as a function of the distance r from center for a tumor with a radius of 1.0 cm, for three different antibodies distribution: Uniform, linear, and exponential. The gray parts symbolize the hypoxic core of 0.64 cm radius and dotted vertical lines represent the tumor radius. Values for BED(r) were determined according to parameters given in Table II and Eq. (5) with $q=1$, with the exception that the value of q changes from 1 to 3 for the hypoxic core.

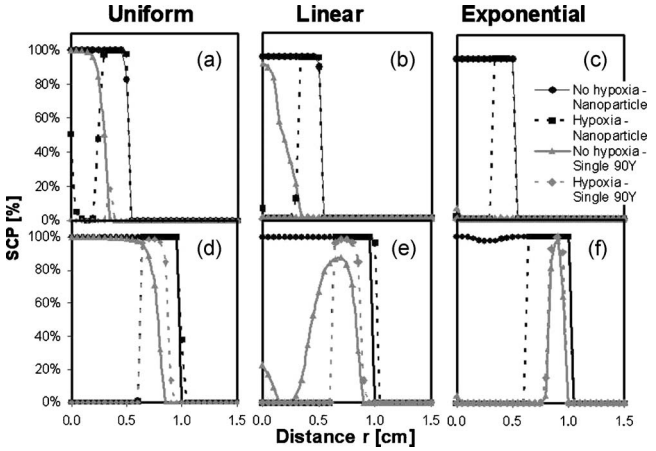

FIG. 7. SCP profiles, in %, as a function of distance r from center of a tumor of 0.5 cm radius [(a)–(c)] and 1.0 cm radius [(d)–(f)] when 5 nm diameter nanoparticles containing $^{90}Y_2O_3$ molecules (black curves) or when single ^{90}Y (gray curves) are linked to antibodies distributed uniformly, linearly and exponentially. Solid and dashed curves correspond, respectively, to BED calculations applied for tumors without hypoxia (solid curve) and when 25% of total cell clusters are hypoxic at the tumor center (dashed curves).

poxic cell clusters compared to the total number of cell aggregates was chosen to be 25%, corresponding to a spherical hypoxic core of 0.32 radius for the smaller carcinoma and of 0.64 cm radius for the largest (cf. Table I). The absorbed and biological dose profiles are calculated with the same total activity as the tumor model without central hypoxia, namely, 3.5 and 20 MBq for 0.5 and 1.0 tumor radii, respectively. When a single radioactive atom of ^{90}Y is linked to each antibody, the total activities decrease to values of 0.9 and 7.5 MBq for 0.5 and 1.0 cm tumor radii, respectively. Distributions of radiolabeled antibodies in the normally oxygenated part of the spherical solid tumor can be uniform, linear, or exponential.

III.B.1. Nanoparticle labeled antibody

Figures 5 and 6 show the impact of poorly oxygenated cells on BED calculation. For the three distributions of radiolabeled antibodies, the shapes between physical dose and BED curves are different. Indeed, biological doses are higher than absorbed doses in the normally oxygenated region of the tumor but lower in the hypoxic core. Maximum values for BED(r) in a tumor of 0.5 cm radius are 162 Gy for uniform distribution and 150 Gy for linear or exponential distribution of radiolabeled antibodies. The aforementioned biological doses are located at a distance varying between 0.30 and 0.40 cm from the tumor center where the proliferation of cells is still important. Higher values for maximal BED are observed when the tumor reaches 1.0 cm radius with 158, 156, and 170 Gy for uniform, linear, and exponential distributions, respectively. These values are localized at 0.70 cm from the tumor center for uniform or linear distribution and at 0.90 for the exponential distribution of activity. As for Figs. 4 and 5, error bars have been added on BED curves and wide variations in biological doses are observed only in the living part of the tumor. Changes in BED are essentially due to fluctuations in the repair half-time since an increase of 40–55 Gy is observed when T_μ is 1.5 h rather than 0.5 h for both tumor radii. Once again, important variations for α/β and μ biological parameters do not affect BED very much: BED(r) remains high inside the nonhypoxic area of the tumor with doses up to 50 Gy, which are values high enough to ensure good treatment outcomes. Inversely, BED values in the hypoxic core are always inferior to 50 Gy with a minimal value of about 20 Gy at the center of the core for the tumor of 0.5 cm radius. The latter is still reduced to values close to zero for larger spherical tumors. BED(r) values in this region are significantly smaller than physical doses when we take into account that hypoxic cells are more radioresistant than oxic cells. Finally, BED values in healthy tissue are about 30 Gy at a distance of 1 mm from the tumor, except for the exponential distribution. In this last case, BED value is higher than 40 Gy, which is too high if we wish to avoid important damage to the lung tissues (or surrounding tissues) in close proximity.

III.B.2. Single atom labeled antibody

Once again, previous results have been compared to D and BED calculations when only a single atom is linked to each antibody. For the tumor of 0.5 cm radius in which 25% of the cell clusters are poorly oxygenated at the center (Fig. 5), maximal doses range from 30 to 35 Gy at 0.35 cm from the tumor center for uniform distribution and at 0.40 cm from the tumor center for linear or exponential antibody distribution. Biological doses lower than 10 Gy are also calculated in the hypoxic core. All these BED values are much too low to eradicate completely the tumor. For a larger tumor of 1.0 cm radius (Fig. 6), maximal doses reached also remain inferior to 60 Gy whatever the antibody distribution and the biological doses are close to zero at the tumor center. It has to be noted that values for absorbed and biological doses

remain inferior to 15 Gy in healthy tissues for both tumor radii and for the three activity distributions, which means that the treatment remains harmless for healthy tissues.

III.C. SCP distributions

Up to now, it is not clear which antibody distribution would be the most efficient to treat spherical solid cancers, such as NSCLC. The only important difference between the three distributions we envisaged is the localization of the maximum of the biologically effective dose inside the tumor that could influence treatment outcome. For uniform distribution, this maximum is located at the tumor center while this maximum shifts near the tumor surface when the distribution becomes exponential. Figure 7 shows shell control probabilities in relation to the distance r for two spherical tumors with radii of 0.5 cm [cf. Figs. 7(a)–7(c)] or 1.0 cm [cf. Figs. 7(d)–7(f)]. SCP(r) has been plotted for non-small-cell lung cancer (α=0.350 Gy^{-1}) surrounded by lung tissues (α=0.031 Gy^{-1}). Uniform [Figs. 7(a) and 7(d)], linear [Figs. 7(b) and 7(e)], or exponential [Fig. 7(c) and 7(f)] distributions caused by uniform or nonuniform antibody uptake are considered.

III.C.1. Nanoparticle labeled antibody

When a NSCLC tumor of 0.5 cm radius does not present a hypoxic core, and when it is treated with 5 nm diameter nanoparticles of $^{90}Y_2O_3$, the SCP curve displays a plateau from the center of the tumor toward its surface and this, independently of the antibody distribution. These results mean that the probability to observe a cell cluster surviving irradiation is very weak throughout the whole tumor. The only difference between the three distributions is the value of SCP at the tumor surface. Indeed, SCP is maximal for exponential antibody distributions and is a little bit lower when antibodies are distributed linearly (SCP of 94%) or uniformly (SCP of 83%). Finally, SCP rapidly decreases to zero in lung healthy tissues, for the three distributions. Tumor control probabilities for uniform, linear, and exponential distributions are, respectively, 83%, 94%, and 100%.

Similar results are obtained when the spherical tumor reaches a radius of 1.0 cm [Figs. 7(d)–7(f)]. SCP values of 100% are calculated inside the tumor, except for the exponential antibody distributions for which a small decrease in SCP from 100% to 97% is observed halfway between the center and the surface of the tumor. Inversely, SCP values of 0% are observed in healthy tissues. At the tumor surface, SCP varies from 100% for the exponential activity to 0% when the radionuclides contained in the nanoparticles are distributed uniformly through the tumor. In general, simulated curves plotted on Fig. 7 indicate that a good treatment outcome could be obtained with the use of radioactive nanoparticles coupled to each antibody, independently of the activity distribution (uniform, linear, or exponential). With 87%, the best TCP is obtained for exponential distribution of antibodies.

Figure 7 also shows values of SCP plotted against r when spherical carcinomas present a hypoxic core, i.e., 25% of the total number of cell clusters is poorly oxygenated at the center of the tumor. In this case, SCP decreases from 100% to 0% in the region of the hypoxic core. This result indicates that the use of 5 nm diameter nanoparticles containing ^{90}Y is not efficient enough to irradiate three times more radioresistant cell clusters when the antibodies cannot penetrate inside this part of the tumor.

We have also investigated the variation in SCP when values of the different biological parameters (α, α/β, N, and μ) vary. Study was made of a plausible range of values, similar to those proposed by Atthey and co-workers.[37] For small tumors of 0.5 cm radius, variation in α/β and μ does not modify SCP values, which means that treatment outcome does not change even with a reasonable fluctuation of BED. For a larger tumor of 1.0 cm radius, similar variations in α/β and μ provoke only very small differences of SCP at the tumor surface. When the cell density varies from 10^7 to 10^8, N changes, but SCP values remains identical for both tumors. The fact that SCP values remain unchanged when α/β, μ, and N vary is the consequence of the high activity released by the nanoparticles. However SCP at the tumor surface increases when α varies from 0.20 to 0.5 Gy^{-1}. For α larger than 0.5 Gy^{-1}, SCP reaches a maximum of 100% at the tumor surface, where cellular proliferation is very important. On the other hand, when α values are lower than 0.20 Gy^{-1}, SCP values at the tumor surface remain zero.

III.C.2. Single atom labeled antibody

As presented by the SCP curves in Fig. 7, when a single ^{90}Y is linked to each antibody, the sizes of tumors, antibody distributions, and the presence of hypoxic cells greatly influence SCP distribution. For example, no cell clusters will be killed when the tumor has a radius of 0.5 cm and presents a central hypoxia of 0.32 cm radius [Figs. 7(a)–7(c)]. Indeed, SCP values of 0% are calculated for all measures of r. Similar results are observed when the tumor has no hypoxic core and an exponential antibody distribution. Consequently, when tumor has a radius of 0.5 cm and no central hypoxia, better therapeutic effects are obtained when antibodies are distributed uniformly or linearly. In these last cases, a SCP of 100% is reached at the tumor center and decreases progressively through the tumor to a value of 0% at 2 mm before the surface. These results lead to the conclusion that the most highly proliferating cells are not sufficiently irradiated to have a chance of a cancer cure.

Figure 7 shows that SCP results for larger tumors of 1.0 cm radius are totally different. Without hypoxia, the shape of SCP curves varies according to the types of antibody distribution. When antibodies are distributed uniformly [Fig. 7(d)], SCP displays a plateau in the center of the tumor and then decreases near the tumor surface which is the region where the number of proliferating cells is the most important. For linear and exponential distributions [Figs. 7(e) and 7(f)], the maximal values of SCP are located, respectively, at a distance of 0.70 and 0.90 cm from the center of the tumor, with a narrower and higher peak for the exponential distribution. Inversely, the shape of SCP curves for the three dif-

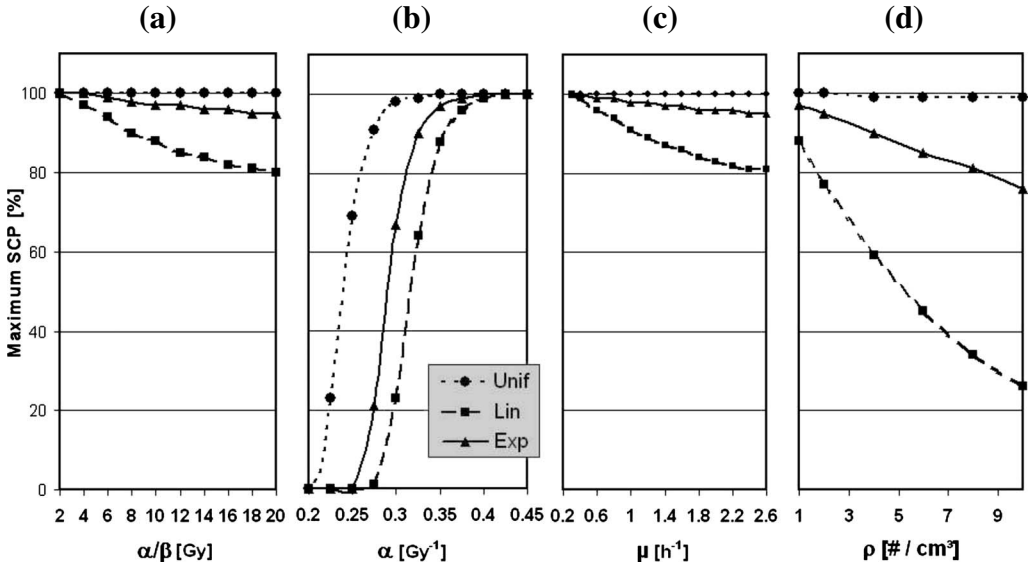

FIG. 8. Variation in maximal SCP values, in %, with the different radiobiological factors: (a) The ratio α/β, (b) the intrinsic radiosensitivity α, (c) the exponential cellular repair constant μ, and (d) the cell density ρ. SCP calculations were performed for a tumor of 1.0 cm without hypoxia and for single ^{90}Y labeled antibodies. Activity inside the tumor may be distributed uniformly (dotted curves), linearly (dashed curves), or exponentially (solid curves).

ferent antibody distributions is similar when the tumor has a hypoxic core. A maximal SCP of 100% is reached in the normally oxygenated part of the tumor, with a deeper radial position within the tumor when the antibodies are uniformly distributed through the tumor. Moreover, the more the distribution is exponential, the more the peak is narrow. A better shell control probability seems to be obtained when the quantity of antibodies decrease linearly through the nonhypoxic part of the 1.0 cm radius tumor.

Variations in the maximal value for SCP were evaluated for a wide range of biological parameters. Figure 8 shows that maximal SCP values obtained for a tumor of 1.0 cm radius without hypoxia decrease when the ratio α/β, the cellular repair constant and the cell density ρ increase. Results also indicate that shell control probability decreases rapidly when the intrinsic radiosensitivity α is lower than 0.35 Gy. Consequently, due to the lower doses deposited inside the tumor when single radionuclides coupled to each antibody is used rather than radioactive nanoparticles, values of SCP depend more on the choice of biological parameters and the antibody distributions.

IV. CONCLUSIONS

In RIT, dose deposition inside the tumor is performed by the use of monoclonal antibodies labeled with only one radioactive atom. In a previous work, the advantage of using radioactive nanoparticles containing hundreds of radioactive atoms rather than single radionuclides was modelized.[6] Dosimetry calculations were performed with the MCNPX Monte Carlo code by introducing a new model of tumor in which radiolabeled antibodies can be uniformly, linearly, or exponentially distributed. However, these deposited doses did not take into account the radiosensitivity and cellular repair effects of the targeted tumor and surrounding tissue. Therefore, BED and SCP formulas were applied in this work to estimate more properly the tumor response and treatment outcome.

BED and SCP distributions were calculated for advanced non-small-cell lung cancer for which no efficacious therapy exists. When only one β-emitter ^{90}Y is coupled to each antibody, the calculated BED is lower than 60 Gy in the overall tumor. SCP values show clearly that these biological doses are insufficient to correctly treat NSCLC. When the single β-emitter is replaced by a 5 nm diameter nanoparticle containing approximately 1000 ^{90}Y atoms, sufficiently high biological doses can be obtained to completely kill the nonhypoxic part of a NSCLC, while limiting radiation in healthy lung tissues. SCP calculations confirm these results by reaching a maximal value of 100% inside the normally oxygenated part of the tumor and a minimal value of 0% in the surrounding healthy tissues. However, BED and SCP values are influenced by the choice of the geometrical factors used to describe the tumor (i.e., morphology of the tumor and cell cluster dimensions, radioactivity distribution throughout the tumor, and volume of hypoxic core) by the model used to calculate BED(r) (i.e., LQ model, cellular repair, and hypoxic and repopulation effects) and by biological parameter values selected for NSCLC and lung tissues. Variability of both SCP and BED distributions have been analyzed for a wide range of biological parameter values and the results confirm their important impact on BED distributions inside the tumor. Inversely, it is interesting to note that despite large differences in BED curves, shell control probability remains relatively unaffected when radioactive nanoparticles are used. This last result is probably due to the high activity deposited inside the tumor by the numerous radioactive atoms contained in the nanoparticles. To conclude this paper, for either small or large solid tumors, BED and SCP calculations clearly confirm the efficacy of radioimmunotherapy when using radioactive nanoparticles rather than a single radionuclide coupled to each antibody.

ACKNOWLEDGMENTS

This research (Targan Project–Convention 0516071) was supported by the Walloon Region (Belgium). Olivier Feron is senior research associate of FNRS (Fonds National de la Recherche Scientifique, Belgium).

[a]Author to whom correspondence should be addressed. Electronic mail: virginie.bouchat@fundp.ac.be; Telephone: 0032-81-725479; Fax: 0032-81-725474.

[1]M. Mehta, R. Scrimger, R. Mackie, B. Paliwal, R. Chappell, and J. Fowler, "A new approach to dose escalation in non-small-cell lung cancer," Int. J. Radiat. Oncol., Biol., Phys. **49**, 23–33 (2001).
[2]W. A. Bethge and B. M. Sandmaier, "Targeted cancer therapy using radiolabeled monoclonal antibodies," Technol. Cancer Res. Treat. **4**, 393–405 (2005).
[3]S. V. Govindan, G. L. Griffiths, H. J. Hansen, I. D. Horak, and D. M. Goldenberg, "Cancer therapy with radiolabeled and drug/toxin-conjugated antibodies," Technol. Cancer Res. Treat. **4**, 375–391 (2005).
[4]R. M. Sharkey and D. M. Goldenberg, "Perspectives on cancer therapy with radiolabeled monoclonal antibodies," J. Nucl. Med. **46**, 115s–127s (2005).
[5]D. M. Goldenberg, "Advancing role of radiolabeled antibodies in the therapy of cancer," Cancer Immunol. Immunother **52**, 281–296 (2003).
[6]V. Bouchat, V. E. Nuttens, S. Lucas, C. Michiels, B. Masereel, O. Feron, B. Gallez, and T. V. Borght, "Radioimmunotherapy with radioactive nanoparticles: First results of dosimetry for vascularized and necrosed solid tumors," Med. Phys. **34**, 4504–4513 (2007).
[7]M. J. Welch, C. J. Hawker, and K. L. Wooley, "The advantages of nanoparticles for PET," J. Nucl. Med. **50**, 1743–1746 (2009).
[8]F. Pene, E. Courtine, A. Cariou, and J. P. Mira, "Toward theragnostics," Crit. Care Med. **37**, S50–S58 (2009).
[9]S. M. Moghimi, A. C. Hunter, and J. C. Murray, "Nanomedicine: Current status and future prospects," FASEB J. **19**, 311–330 (2005).
[10]S. M. Moghimi and J. Szebeni, "Stealth liposomes and long circulating nanoparticles: Critical issues in pharmacokinetics, opsonization and protein-binding properties," Prog. Lipid Res. **42**, 463–478 (2003).
[11]D. E. Owens III and N. A. Peppas, "Opsonization, biodistribution, and pharmacokinetics of polymeric nanoparticles," Int. J. Pharm. **307**, 93–102 (2006).
[12]R. Gref, M. Luck, P. Quellec, M. Marchand, E. Dellacherie, S. Harnisch, T. Blunk, and R. H. Muller, "'Stealth' corona-core nanoparticles surface modified by polyethylene glycol (PEG): Influences of the corona (PEG chain length and surface density) and of the core composition on phagocytic uptake and plasma protein adsorption," Colloids Surf., B **18**, 301–313 (2000).
[13]Y. Yi, J. H. Kim, H. W. Kang, H. S. Oh, S. W. Kim, and M. H. Seo, "A polymeric nanoparticle consisting of mPEG-PLA-Toco and PLMA-COONa as a drug carrier: Improvements in cellular uptake and biodistribution," Pharm. Res. **22**, 200–208 (2005).
[14]J. Chen, H. Wu, D. Han, and C. Xie, "Using anti-VEGF McAb and magnetic nanoparticles as double-targeting vector for the radioimmunotherapy of liver cancer," Cancer Lett. **231**, 169–175 (2006).
[15]G. Kaul and M. Amiji, "Biodistribution and targeting potential of poly(ethylene glycol)-modified gelatin nanoparticles in subcutaneous murine tumor model," J. Drug Target. **12**, 585–591 (2004).
[16]J. D. Woodward, S. J. Kennel, S. Mirzadeh, S. Dai, J. S. Wall, T. Richey, J. Avenell, and A. J. Rondinone, "In vivo SPECT/CT imaging and biodistribution using radioactive (CdTe)-Te-125m/ZnS nanoparticles," Nanotechnology **18**, 175103 (2007).
[17]R. Kannan, V. Rahing, C. Cutler, R. Pandrapragada, K. K. Katti, V. Kattumuri, J. D. Robertson, S. J. Casteel, S. Jurisson, C. Smith, E. Boote, and K. V. Katti, "Nanocompatible chemistry toward fabrication of target-specific gold nanoparticles," J. Am. Chem. Soc. **128**, 11342–11343 (2006).
[18]K. V. Katti, R. Kannan, K. Katti, V. Kattumori, R. Pandrapraganda, V. Rahing, C. Cutler, E. J. Boote, S. W. Casteel, C. J. Smith, J. D. Robertson, and S. S. Jurrison, "Hybrid gold nanoparticles in molecular imaging and radiotherapy," Czech. J. Phys. **56**, D23–D34 (2006).
[19]N. Chanda *et al.*, "Radioactive gold nanoparticles in cancer therapy: Therapeutic efficacy studies of (198)AuNP-GA nanoconstruct in prostate tumor-bearing mice," Nanomedicine (in press).
[20]H. Wu, J. Wang, Z. Wang, D. R. Fisher, and Y. Lin, "Apoferritin-templated yttrium phosphate nanoparticle conjugates for radioimmunotherapy of cancers," J. Nanosci. Nanotechnol. **8**, 2316–2322 (2008).
[21]D. D. Dionysiou and G. S. Stamatakos, "Applying a 4D multiscale in vivo tumor growth model to the exploration of radiotherapy scheduling: The effects of weekend treatment gaps and p53 gene status on the response of fast growing solid tumors," Cancer Inform. **2**, 113–121 (2006).
[22]R. Ruggieri, "Hypofractionation in non-small cell lung cancer (NSCLC): Suggestions from modeling both acute and chronic hypoxia," Phys. Med. Biol. **49**, 4811–4823 (2004).
[23]D. Levin-Plotnik and R. J. Hamilton, "Optimization of tumour control probability for heterogeneous tumours in fractionated radiotherapy treatment protocols," Phys. Med. Biol. **49**, 407–424 (2004).
[24]M. G. Stabin and G. D. Flux, "Internal dosimetry as a tool for radiation protection of the patient in nuclear medicine," Biomed. Imaging Interv. J. **3**, e28 (2007).
[25]M. G. Stabin, M. Tagesson, S. R. Thomas, M. Ljungberg, and S. E. Strand, "Radiation dosimetry in nuclear medicine," Appl. Radiat. Isot. **50**, 73–87 (1999).
[26]R. Barone, F. O. Borson-Chazot, R. Valkerna, S. Walrand, F. Chauvin, L. Gogou, L. K. Kvols, E. P. Krenning, F. Jamar, and S. Pauwels, "Patient-specific dosimetry in predicting renal toxicity with Y-90-DOTATOC: Relevance of kidney volume and dose rate in finding a dose-effect relationship," J. Nucl. Med. **46**, 99s–106s (2005).
[27]M. Astrahan, "Some implications of linear-quadratic-linear radiation dose-response with regard to hypofractionation," Med. Phys. **35**, 4161–4172 (2008).
[28]B. Warkentin, P. Stavrev, N. Stavreva, C. Field, and B. Fallone, "A TCP-NTCP estimation module using DVHs and known radiobiological models and parameter sets," J. Appl. Clin. Med. Phys. **5**, 50–63 (2004).
[29]P. Thirion, O. Holmberg, C. D. Collins, C. O'Shea, M. Moriarty, M. Pomeroy, C. O'Sullivan, S. Buckney, and J. Armstrong, "Escalated dose for non-small-cell lung cancer with accelerated hypofractionated three-dimensional conformal radiation therapy," Radiother. Oncol. **71**, 163–166 (2004).
[30]E. Kodym, R. Kodym, A. E. Reis, A. A. Habib, M. D. Story, and D. Saha, "The small-molecule CDK inhibitor, SNS-032, enhances cellular radiosensitivity in quiescent and hypoxic non-small cell lung cancer cells," Lung Cancer **66**, 37–47 (2009).
[31]M. Engelsman, E. M. Damen, K. De Jaeger, K. M. van Ingen, and B. J. Mijnheer, "The effect of breathing and set-up errors on the cumulative dose to a lung tumor," Radiother. Oncol. **60**, 95–105 (2001).
[32]B. Döme, S. Paku, B. Somlai, and J. Timar, "Vascularization of cutaneous melanoma involves vessel co-option and has clinical significance," J. Pathol. **197**, 355–362 (2002).
[33]J. A. M. Beliën, P. J. van Diest, and J. P. A. Baak, "Relationships between vascularization and proliferation in invasive breast cancer," J. Pathol. **189**, 309–318 (1999).
[34]C. Schlueter, H. Weber, B. Meyer, P. Rogalla, K. Roser, S. Hauke, and J. Bullerdiek, "Angiogenetic signaling through hypoxia-HMGB1: An angiogenetic switch molecule," Am. J. Pathol. **166**, 1259–1263 (2005).
[35]J. L. Humm and L. M. Cobb, "Nonuniformity of tumor dose in radioimmunotherapy," J. Nucl. Med. **31**, 75–83 (1990).
[36]V. E. Nuttens, A. C. Wera, V. Bouchat, and S. Lucas, "Determination of biological vector characteristics and nanoparticle dimensions for radioimmunotherapy with radioactive nanoparticles," Appl. Radiat. Isot. **66**, 168–172 (2008).
[37]M. Atthey, A. E. Nahum, M. A. Flower, and V. R. McCready, "Effects of cellular repair and proliferation on targeted radionuclide therapy: A modeling study," Phys. Med. Biol. **45**, N15–N20 (2000).
[38]M. Cremonesi, M. Ferrari, L. Bodei, G. Tosi, and G. Paganelli, "Systemic and locoregional dosimetry in receptor radionuclide therapy with peptides," Q. J. Nucl. Med. Mol. Imaging **50**, 288–295 (2006).
[39]R. W. Howell, D. V. Rao, and K. S. R. Sastry, "Macroscopic dosimetry for radioimmunotherapy-nonuniform activity distributions in solid tumors," Med. Phys. **16**, 66–74 (1989).
[40]R. M. Sharkey and D. M. Goldenberg, "Use of antibodies and immunoconjugates for the therapy of more accessible cancers," Adv. Drug Delivery Rev. **60**, 1407–1420 (2008).
[41]G. A. Wiseman, C. A. White, R. B. Sparks, W. D. Erwin, D. A. Podoloff, D. Lamonica, N. L. Bartlett, J. A. Parker, W. L. Dunn, S. M. Spies, R. Belanger, T. E. Witzig, and B. R. Leigh, "Biodistribution and dosimetry results from a phase III prospectively randomized controlled trial of Zeva-

lin (TM) radioimmunotherapy for low-grade, follicular, or transformed B-cell non-Hodgkin's lymphoma," Crit. Rev. Oncol. Hematol. **39**, 181–194 (2001).
[42]R. W. Howell, S. M. Goddu, and D. V. Rao, "Application of the linear-quadratic model to radioimmunotherapy-further support for the advantage of longer-lived radionuclides," J. Nucl. Med. **35**, 1861–1869 (1994).
[43]K. Tobinai, Y. Kobayashi, M. Narabayashi, M. Ogura, Y. Kagami, Y. Morishima, T. Ohtsu, T. Igarashi, Y. Sasaki, T. Kinoshita, and T. Murate, "'Feasibility and pharmacokinetic study of a chimeric anti-CD20 monoclonal antibody (IDEC-C2B8, rituximab) in relapsed B-cell lymphoma,' The IDEC-. C2B8 Study Group," Ann. Oncol. **9**, 527–534 (1998).
[44]N. Reynaert, H. Palmans, H. Thierens, and R. Jeraj, "Parameter dependence of the MCNP electron transport in determining dose distributions," Med. Phys. **29**, 2446–2454 (2002).
[45]D. R. Schaart, J. T. Jansen, J. Zoetelief, and P. F. de Leege, "A comparison of MCNP4C electron transport with ITS 3.0 and experiment at incident energies between 100 keV and 20 MeV: Influence of voxel size, substeps and energy indexing algorithm," Phys. Med. Biol. **47**, 1459–1484 (2002).
[46]B. Brans, L. Bodei, F. Giammarile, O. Linden, M. Luster, W. J. G. Oyen, and J. Tennvall, "Clinical radionuclide therapy dosimetry: The quest for the 'Holy Gray'," Eur. J. Nucl. Med. Mol. Imaging **34**, 772–786 (2007).
[47]R. G. Dale, "The application of the linear-quadratic dose-effect equation to fractionated and protracted radiotherapy," Br. J. Radiol. **58**, 515–528 (1985).
[48]R. Dale and A. Carabe-Fernandez, "The radiobiology of conventional radiotherapy and its application to radionuclide therapy," Cancer Biother. Radiopharm. **20**, 47–51 (2005).
[49]R. K. Bodey, P. M. Evans, and G. D. Flux, "Application of the linear-quadratic model to combined modality radiotherapy," Int. J. Radiat. Oncol., Biol., Phys. **59**, 228–241 (2004).
[50]C. Chiesa, F. Botta, E. Di Betta, A. Coliva, M. Maccauro, G. Aliberti, S. Bavusi, L. Devizzi, A. Guidetti, E. Seregni, A. M. Gianni, and E. Bombardieri, "Dosimetry in myeloablative Y-90-labeled ibritumomab tiuxetan therapy: Possibility of increasing administered activity on the base of biological effective dose evaluation. Preliminary results," Cancer Biother. Radiopharm. **22**, 113–120 (2007).
[51]S. Baechler, R. F. Hobbs, A. R. Prideaux, R. L. Wahl, and G. Sgouros, "Extension of the biological effective dose to the MIRD schema and possible implications in radionuclide therapy dosimetry," Med. Phys. **35**, 1123–1134 (2008).
[52]J. Z. Wang, X. A. Li, W. D. D'Souza, and R. D. Stewart, "Impact of prolonged fraction delivery times on tumor control: A note of caution for intensity-modulated radiation therapy (IMRT)," Int. J. Radiat. Oncol., Biol., Phys. **57**, 543–552 (2003).
[53]G. G. Steel, J. M. Deacon, G. M. Duchesne, A. Horwich, L. R. Kelland, and J. H. Peacock, "The dose-rate effect in human-tumor cells," Radiother. Oncol. **9**, 299–310 (1987).
[54]M. Guerrero and X. A. Li, "Halftime for repair of sublethal damage in normal bladder and rectum: An analysis of clinical data from cervix brachytherapy," Phys. Med. Biol. **51**, 4063–4071 (2006).
[55]A. Dawson and T. Hillen, "Derivation of the tumour control probability (TCP) from a cell cycle model," Comput. and Math. Meth. in Medicine **7**, 121–141 (2006).
[56]N. Matsufuji, T. Kanai, N. Kanematsu, T. Miyamoto, M. Baba, T. Kamada, H. Kato, S. Yamada, J. E. Mizoe, and H. Tsujii, "Specification of carbon ion dose at the National Institute of Radiological Sciences (NIRS)," J. Radiat. Res. (Tokyo) **48**, A81–A86 (2007).
[57]R. G. Dale, "Dose-rate effects in targeted radiotherapy," Phys. Med. Biol. **41**, 1871–1884 (1996).
[58]J. F. Fowler, "Development of radiobiology for oncology-a personal view," Phys. Med. Biol. **51**, R263–R286 (2006).
[59]R. Dale and C. Deehan, "Brachytherapy," in *Radiobiological Modeling in Radiation Oncology*, edited by R. G. D. B. Jones (The British Institute of Radiology, London, 2007), pp. 113–137.
[60]S. Webb and A. E. Nahum, "A model for calculating tumour control probability in radiotherapy including the effects of inhomogeneous distributions of dose and clonogenic cell density," Phys. Med. Biol. **38**, 653–666 (1993).
[61]B. Dubray, M. Henryamar, J. H. Meerwaldt, E. M. Noordijk, D. O. Dixon, J. M. Cosset, and H. D. Thames, "Radiation-induced lung damage after thoracic irradiation for Hodgkin's disease—The role of fractionation," Radiother. Oncol. **36**, 211–217 (1995).
[62]B. Jones, A. Carabe-Fernandez, and R. Dale, "The oxygen effect," in *Radiobiological Modeling in Radiation Oncology*, edited by R. G. D. B. Jones (The British Institute of Radiology, London, 2007), Vol. 1, pp. 138–157.
[63]R. D. Stewart and R. J. Traub, "Radiobiological modeling in voxel constructs," presented at the *Proceedings of the Monte Carlo 2000 Meeting*, Lisbon, Portugal, 2000, edited by F. B. A. Kling, M. Nakagawa, L. Tavora, and P. Vaz (Springer-Verlag, Berlin, 2001), pp. 285–290.